

Journal of Vertebrate Paleontology

ISSN: 0272-4634 (Print) 1937-2809 (Online) Journal homepage: www.tandfonline.com/journals/ujvp20

Re-evaluating the Plagne (Tithonian) theropod trackway: quantitative analyses provide evidence on the presence of *Megalosauripus transjuranicus* in the French Jura

Vincenzo Gesualdi, Lara Sciscio, Christian A. Meyer, Alessandro Riga, Diego Castanera, Emmanuel Fara, Jean-David Moreau & Matteo Belvedere

To cite this article: Vincenzo Gesualdi, Lara Sciscio, Christian A. Meyer, Alessandro Riga, Diego Castanera, Emmanuel Fara, Jean-David Moreau & Matteo Belvedere (25 Aug 2026): Re-evaluating the Plagne (Tithonian) theropod trackway: quantitative analyses provide evidence on the presence of *Megalosauripus transjuranicus* in the French Jura, Journal of Vertebrate Paleontology, DOI: 10.1080/02724634.2026.2710193

To link to this article: https://doi.org/10.1080/02724634.2026.2710193

© 2026 Vincenzo Gesualdi, Lara Sciscio, Christian A. Meyer, Alessandro Riga, Diego Castanera, Emmanuel Fara, Jean-David Moreau, and MatteoBelvedere

Published online: 25 Aug 2026.

Submit your article to this journal

Article views: 796

View related articles

View Crossmark data

Full Terms & Conditions of access and use can be found at
https://www.tandfonline.com/action/journalInformation?journalCode=ujvp20

Journal of Vertebrate Paleontology e2710193 (17 pages)
Published with license by the Society of Vertebrate Paleontology
DOI: 10.1080/02724634.2026.2710193

Check for updates

ARTICLE

RE-EVALUATING THE PLAGNE (TITHONIAN) THEROPOD TRACKWAY: QUANTITATIVE ANALYSES PROVIDE EVIDENCE ON THE PRESENCE OF *MEGALOSAURIPUS TRANSJURANICUS* IN THE FRENCH JURA

VINCENZO GESUALDI, [1*] LARA SCISCIO, [2,3] CHRISTIAN A. MEYER, [4] ALESSANDRO RIGA, [5] DIEGO CASTANERA, [6] EMMANUEL FARA, [7] JEAN-DAVID MOREAU, [8] and MATTEO BELVEDERE [1]
[1]Dipartimento di Scienze della Terra, Università degli Studi di Firenze, Firenze, 50121, Italy, vincenzo.gesualdi@unifi.it; matteo.belvedere@unifi.it;
[2]JURASSICA Museum, Porrentruy, CH-2900, Switzerland, lara.sciscio@jurassica.ch;
[3]Department of Geosciences, University of Fribourg, Fribourg, 1700, Switzerland;
[4]Department of Environmental Sciences, University of Basel, Basel, 4056, Switzerland, chris.meyer@unibas.ch;
[5]Department of Biology, University of Florence, Firenze, 50019, Italy, alessandro.riga@unifi.it;
[6]Grupo Aragosaurus-IUCA, Paleontología, Facultad de Ciencias, Universidad de Zaragoza, Zaragoza, 50009, Spain, dcasta@unizar.es;
[7]Université Bourgogne Europe, CNRS, Biogéosciences UMR 6282, Dijon, 21000, France, emmanuel.fara@u-bourgogne.fr;
[8]Université Paris-Saclay, CNRS, GEOPS, Orsay, 91405, France, jean.david.moreau@gmail.com

ABSTRACT—The Upper Jurassic (Oxfordian–Tithonian) carbonate platforms of the Jura region (France and Switzerland) are key to understanding dinosaur ichnology. This record is notable for both the abundance and exceptional preservation of the tracks, which provide valuable insights for ichnotaxonomic analyses and classification. The Plagne tracksite from the Tithonian of the French Jura, preserves numerous tracks of both theropods and sauropods, including the *Brontopodus plagnensis* type trackway, and their exceptional preservation enables detailed and quantitative studies. This study quantitatively tests the hypothesis that the theropod trackway PGN02, from the Plagne tracksite, can be assigned to the ichnospecies *Megalosauripus transjuranicus*. Two quantitative approaches were used: Whole-Track Analysis and two-dimensional geometric morphometrics. Both methods indicate a close morphological affinity between PGN02 and *M. transjuranicus*, and a distinction from other large theropod ichnotaxa (e.g., *Eubrontes*, *Jurabrontes*). The observed differences between PGN02 and the *M. transjuranicus* holotype are interpreted as size-related shape variation, suggesting that the PGN02 trackmaker was a smaller individual than the one that created the holotype, potentially reflecting ontogenetic variation. Plagne's PGN02 tracks extend the geographic range of *M. transjuranicus* to the Tithonian of the French Jura, reinforcing the widespread presence of its trackmaker in Late Jurassic Laurasian ecosystems.

Citation for this article: Gesualdi, V., Sciscio, L., Meyer, C., A. Riga, A., Castanera, D., Fara, E., Moreau, J.-D., & Belvedere, M. (2026) Re-evaluating the Plagne (Tithonian) theropod trackway: Quantitative analyses provide evidence on the presence of *Megalosauripus transjuranicus* in the French Jura. *Journal of Vertebrate Paleontology*. https://doi.org/10.1080/02724634.2026.2710193

Submitted: November 28, 2025
Revisions received: June 6, 2026
Accepted: July 16, 2026

INTRODUCTION

Dinosaur tracks are relatively common in the Upper Jurassic (Oxfordian–Tithonian) of western Europe (e.g., Portugal, France, Switzerland, and Germany), especially in carbonate platforms (D'Orazi Porchetti et al., 2016). Their presence in the Jura Region (France and Switzerland) has been known for decades (Meyer & Lockley, 1996). Both Switzerland (Marty, 2008; Marty et al., 2007; Marty et al., 2018; Meyer & Lockley, 1996; Meyer & Thüring, 2003; Razzolini et al., 2017) and France (Le Loeuff et al., 2006; Mazin et al., 2016; Mazin et al., 2017; Sciscio et al., 2025) have recorded a significant number of tracksites. The paleogeography of the area during the Late Jurassic included several isolated, and relatively small landmasses surrounded by the Tethys Ocean at a paleolatitude estimated to range from 26–27°N (Dercourt et al., 1993). Sea level changes and cyclic platform emersions led to connections between landmasses (Colombié & Strasser, 2005; Enay, 2000; Hallam, 2001; Haq et al., 1987; Jank, Meyer et al., 2006; Jank et al., 2006; Strasser, 2022; Waite et al., 2013), allowing vertebrates to disperse across these corridors (Belvedere et al., 2019; Meyer, 2011). Evidence of landmass emersion is indicated by tidal or supratidal facies, sedimentary structures, and rhizomorphs (Jank, Meyer,

*Corresponding author.
© 2026 Vincenzo Gesualdi, Lara Sciscio, Christian A. Meyer, Alessandro Riga, Diego Castanera, Emmanuel Fara, Jean-David Moreau, and MatteoBelvedere. This is an Open Access article distributed under the terms of the Creative Commons Attribution License (http://creativecommons.org/licenses/by/4.0/), which permits unrestricted use, distribution, and reproduction in any medium, provided the original work is properly cited. The terms on which this article has been published allow the posting of the Accepted Manuscript in a repository by the author(s) or with their consent.

Color versions of one or more of the figures in the article can be found online at www.tandfonline.com/ujvp.

Published online 25 Aug 2026

et al., 2006), as well as terrestrial vertebrate traces that generally occur at the culmination of shallowing-upward cycles (Meyer & Marty, 2014). Thousands of sauropod and theropod tracks occur in the Jura platforms and have led to the recent definition of a few new dinosaurian ichnotaxa: *Jurabrontes curtedulensis* (Marty et al., 2018) and *Megalosauripus transjuranicus* (Razzolini et al., 2017) for theropods, and *Brontopodus plagnensis* (Mazin et al., 2017) for sauropods. In addition to their ichnotaxonomic value, the large number of tracks allow for consistent quantitative analyses to be performed and the validation and application of new research methods (e.g., Belvedere et al., 2018; Castanera et al., 2018; Sciscio et al., 2022).

Megalosauripus represents a significant group of theropod tracks, which are pivotal in understanding the distribution of large-sized theropods, especially during the Middle to Late Jurassic. The nomenclatural history of these tracks is complex, characterized by a prolonged debate (Lockley, Meyer, & dos Santos, 1996, 1998; Thulborn, 2001) that led to the selection of *Megalosauripus* (over *Megalosauropus*) as the valid ichnogenus for Jurassic tracks (Foster et al., 2024; Razzolini et al., 2017). *Megalosauripus* is diagnosed as a medium to large tridactyl theropod ichnogenus. Tracks that can be assigned to it range from 39–72 cm in length and 29–65 cm in width, exhibit a 2-3-4 phalangeal pad impression formula (Foster et al., 2024). The tracks tend to be asymmetric, with the posterior end of the impression of digit III often aligning with the penultimate digital pad impression of digit IV along the anteroposterior axis. Trackways show significant variability in width and pace angulation (Foster et al., 2024; Lockley, Meyer, & dos Santos, 1996, 1998). According to Razzolini et al. (2017), two ichnospecies of *Megalosauripus* are currently considered valid: *Megalosauripus uzbekistanicus* found in the Upper Jurassic of Central Asia (Gabuniya & Kurbatov, 1982; Lockley et al., 1996; Meyer & Lockley, 1997) and *M. transjuranicus* found in the Upper Jurassic of Switzerland (Razzolini et al., 2017). In addition, tracks assigned to *Megalosauripus* cf. *transjuranicus* have been identified in Spain, Portugal, and Morocco (Belvedere et al., 2019; Castanera et al., 2021; Castanera et al., 2023).

This study focuses on a trackway of 10 theropod footprints (PGN02) from the Upper Jurassic (Tithonian) of Plagne, Ain Department, France (Fig. 1). These tracks were originally described by Mazin et al. (2017), who only assigned them to *Megalosauripus*. The original excavation revealed a total of 18 tracks, eight of which, laying outside the protective shelter, are now covered for conservation reasons. Not only is PGN02 the only theropod trackway from the Plagne tracksite, it is also of great importance due to its high level of preservation. All the main track features (digital impressions, pad impressions, and claw mark impressions) are visible, so perhaps a classification at the ichnospecies level can be achieved. Given the integrity of tracks being uncompromised it was possible to apply quantitative methods such as Whole-Track Analysis (WTA) and geometric morphometrics (GM) to PGN02 to ensure a robust ichnotaxonomic assignment and validate whether the trackway can be assigned to *Megalosauripus*, and specifically, *M. transjuranicus*.

Geological Setting

Theropod trackway (PGN02) occurs at tracksite near the village of Plagne (Ain Department, France), which is managed by the Dinoplagne museum (Fig. 1). Tracks of both sauropod and theropod occur at this stie, which is in the Tithonian Couches du Chailley Formation (Bernier, 1984). This formation consists of bioturbated limestones, often encrusted at the base with the oyster *Nanogyra virgula* (Bernier, 1984). The succession is characterized by subtidal to supratidal facies (Mangold & Enay, 2004; Mazin et al., 2017), with dinosaur tracks found in the lower intertidal part (F4 facies, Mazin et al., 2017). At Plagne, tracks occur in three different stratigraphic levels (Fig. 2): the stratigraphically lower-most track-bearing level has tracks only in cross section; the middle track-bearing level

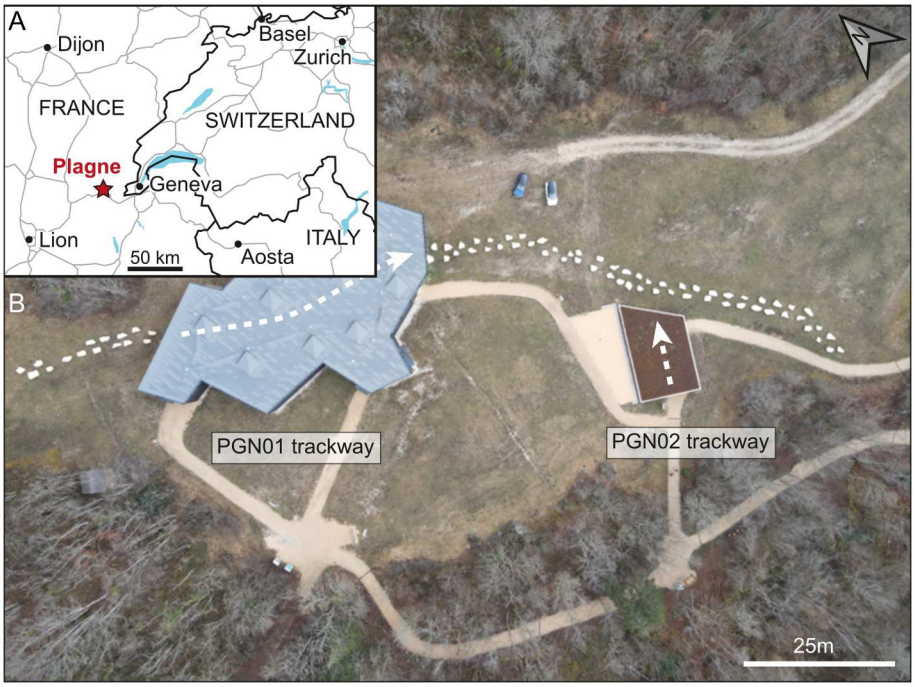


FIGURE 1. **A**, geographic map showing the position of the Plagne tracksite; **B**, aerial view of the Plagne tracksite.

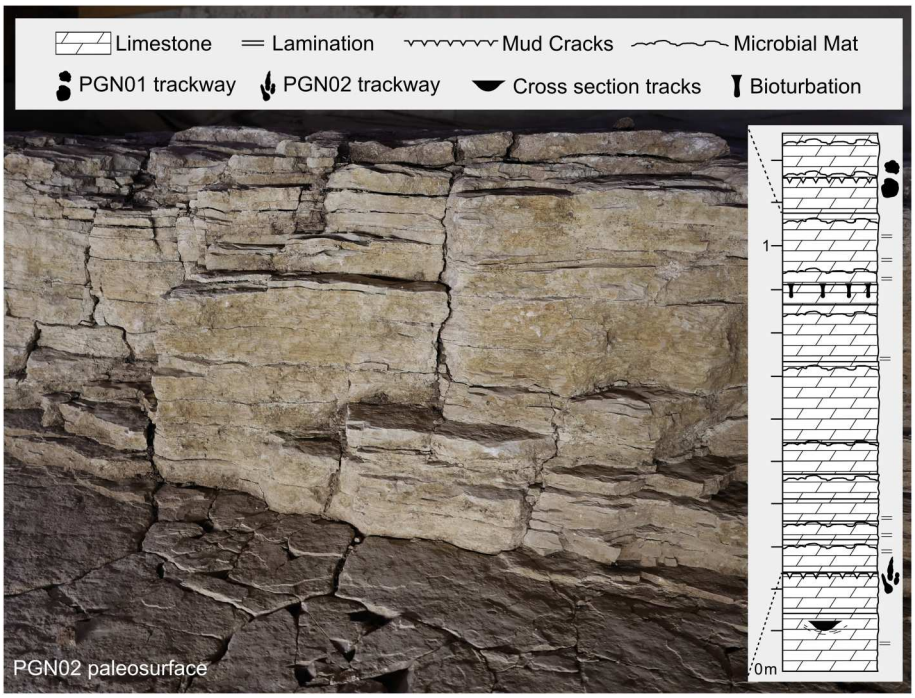


FIGURE 2. Stratigraphic log of the Plagne tracksite showing the track-bearing surfaces.

corresponds to the one with theropod tracks (trackway PGN02), and the upper-most track-bearing level contains the type series of *B. plagnensis* (trackway PGN01). Mazin et al. (2017) proposed a Tithonian age for the Plagne tracksite based on lithostratigraphic correlations between the Couches du Chailley Formation and La Dôle section of the Twannbach Formation, with the Plagne tracksite situated within the *Fallauxi* biozone (Mazin et al., 2017). Sciscio et al. (2025) reported the finding of *Progeronia bruntrutense* (Comment et al., 2015) at the nearby tracksite of Villette. This ammonite is referred to the *Mutabilis* zone, giving a upper Kimmeridgian age to that site (Mangold & Enay, 2004; Sciscio et al., 2025). The Villette tracksite is stratigraphically lower than the Plagne tracksite (Sciscio et al., 2025), thus supporting a younger Tithonian age for Plagne.

MATERIALS AND METHODS

PGN02 comprises a single trackway of 10 sequential theropod tracks (Fig. 3). Tracks were labeled using a combination of the trackway label PGN02, given by Mazin et al. (2017), in addition to the type of tracks ('R' for right and 'L' for left) and a progressive numbering along the trackway (e.g., Marty, 2008). For example, 'PGN02-R1' represents the first right track of the PGN02 trackway.

Tracks and trackway parameters were re-measured in the field (Table 1) following Lallensack et al. (2025), Leonardi (1987), and Thulborn (1990). The size of the tracks follows Marty et al.'s (2018) classification based on the footprint length (FL). Trackmaker speed has been estimated using Alexander's (1976) formula based on hip height calculated according to Thulborn (1990). Measurements (Table 1) have been taken for: footprint length, footprint width (FW), length and width of digits (dII; dIII; dIV; wII; wIII; wIV), interdigital angles (II ^ III; III ^ IV; II ^ IV), anterior triangle (AT), digit III projection (te) and mesaxony (AT l/FW sensu Lockley, 2009). For trackway parameters (S, stride; P, pace length), measurements were taken from the distal end of the third digit, which served as a reference point. The values are reported alongside the corresponding track (e.g., stride between PGN02-R1 and PGN02-L2 is listed in the row for PGN02-L2; Table 1). Tracks were digitized through close-range photogrammetry (Lallensack et al., 2022, Mallison & Wings, 2014) using a Canon EOS R8 (24 Mpixel Full Frame sensor), equipped with a RF 15-30 mm IS STL lens. The 3D models were built using Agisoft Metashape Pro (v. 2.2.2; Agisoft LLC, 2024).

Whole-Track Analysis

Whole-Track Analysis was done using DigTrace (v. 1.8.1; Budka, Bakirov, Deng, et al., 2016; Budka, Bakirov, Falkingham, et al., 2016). The 10 tracks of PGN02 (Fig. 3) were compared with the holotype of *M. transjuranicus* (TCH1030-T6-L1; Razzolini et al., 2017) to quantitatively evaluate the ichnotaxonomic affinity proposed by Mazin et al. (2017) and Razzolini et al. (2017). *Megalosauripus transjuranicus* was chosen as the ichnotaxon also based on the strong morphological similarities with the PGN02 tracks, more than to any other ichnotaxa. The 3D models of each of the 10 tracks of PGN02 trackway were derived from the 3D model of the whole trackway available in the Supplementary Materials (see Data Availability Statement). In DigTrace, landmarks for alignment were placed on the 3D models of tracks (Fig. 4) and then these landmarks are used as anchoring points to overlap two 3D models and measure their degree of similarity. In both cases, the comparison was done choosing Rigid Transformation (no distortion of the tracks). Unfortunately, a stat-track (sensu Belvedere et al., 2018) could not be generated for the PGN02 due to continuous crashes of the software DigTrace. Consequently, a comparison with the *M. transjuranicus* 'mediotype' from Belvedere et al. (2019) was not possible. Our comparisons are restricted to



FIGURE 3. **A**, photographs of all the studied individual tracks from PGN02 trackway; **B**, depth map of the PGN02 trackway. Scale bar equals 35 cm.

TABLE 1. Track and trackway measurements of the Plagne theropod trackway PGN02. **Abbreviations**: see Anatomical Abbreviations in Materials and Methods; **PGN**, Plagne tracksite, Plagne France; **Speed**, trackmaker speed.

Track	FL (cm)	FW (cm)	FL/ FW	dII (cm)	dIII (cm)	dIV (cm)	wII (cm)	wIII (cm)	wIV (cm)	II ^ III (°)	III ^ IV (°)	II ^ IV (°)	P (cm)	S (cm)	AT l/ FW	h (cm)	Speed (km/h)
PGN02-R1	33	16.5	2	12	22.3	14.2	4	6.5	6.2	19	16	35			0.88	161.7	
PGN02-L2	30.5	18.4	1.7	14	20	12	6.5	7.7	5.3	21	23	44	110		0.55	149.5	
PGN02-R2	30	17	1.8	11	19.2	13	6	6	6	26	24	50	111	221	0.87	147	6.7
PGN02-L3	32	19.8	1.6	12	18.6	12	6.5	7.5	4.2	25	26	51	111	222	0.48	156.8	6.3
PGN02-R3	31.5	16.5	1.9	12	21	14	4.5	6.8	5.5	24	26	50	110.5	221	0.72	154.4	6.4
PGN02-L4	32.5	16.5	2	12	19.5	14	4	6.8	4	26	24	50	113	222	0.64	159.3	6.2
PGN02-R4	30.5	17	1.8	12	18	12	5	6.5	6	26	25	51	110	219	0.75	149.5	6.5
PGN02-L5	33	18.5	1.8	11.5	21	12.5	5.5	6.5	4	26	26	52	112	218	0.52	161.7	5.9
PGN02-R5	31	17.5	1.8	12.5	18.4	13.5	4.6	7.5	6.8	26	25	51	109	219	0.85	151.9	6.4
PGN02-L6	32.5	18.5	1.8	12.5	13.6	14	4.5	5.7	5.5	27	25	52	112	220	0.78	159.3	6.1
mean	31.6	17.6	1.8	12.1	19.1	13.1	5.1	6.7	5.3	24.6	24	48.6	111	220	0.7	155	6.3

the holotype of *M. transjuranicus* (TCH1030-T6-L1, Razzolini et al., 2017) in addition to the holotype of *Asianopodus wangi* (LS-T6-R3; Xing et al., 2021). The latter comparison was prompted by the strong similarities observed during geometric morphometrics analyses (see Geometric Morphometrics Results and Discussion sections). These comparisons aim to evaluate similarities among the tracks and to refine the classification of the PGN02 tracks.

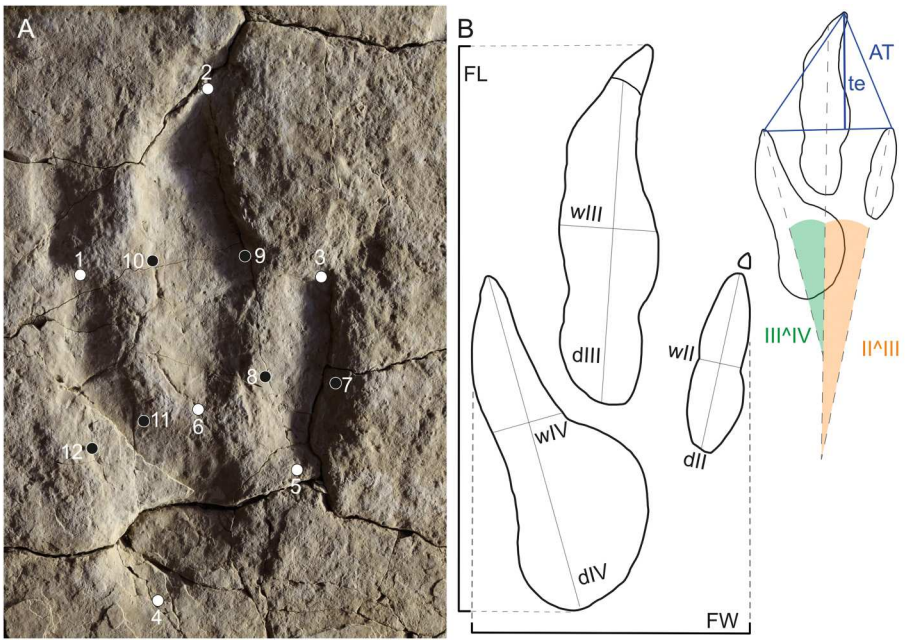


FIGURE 4. **A**, PGN02-R4 track showing the landmarks used in the geometric morphometrics and Whole-Track Analysis. Landmarks were placed at the tips of the impressions of digits II, III, and IV, the posterior margins of the impressions of digits II and IV, the base of the impression of digit III, and width of the impression of digits II, III, and IV. **B**, main measurements taken for the PGN02 tracks. Footprint length is measured along the anteroposterior axis from the 'heel' impression margin to the tip of the impression of digit III. Footprint width is measured along the mediolateral axis between the impression of digits II and IV. All measurements are reported in Table 1. **Abbreviations**: see Anatomical Abbreviations in Materials and Methods.

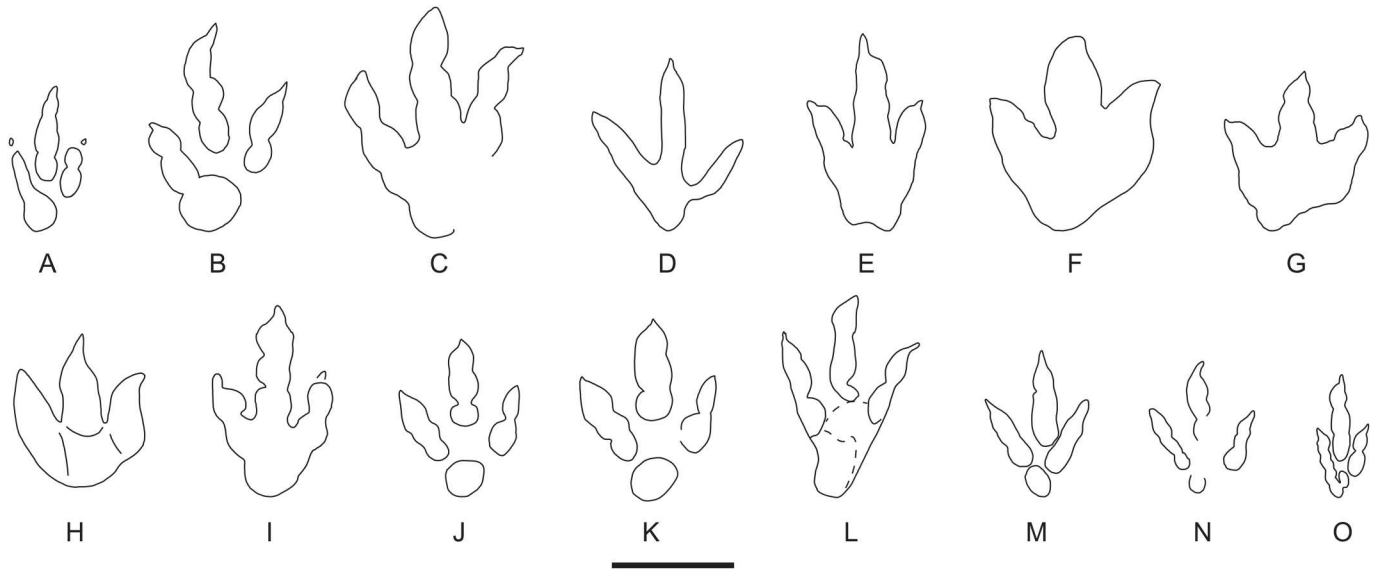


FIGURE 5. Outline drawings of the theropod ichnotaxa used in the geometric morphometrics analyses. **A**, PGN02; **B**, *Megalosauripus transjuranicus* redrawn from Razzolini et al. (2017); **C**, *Megalosauripus uzbekistanicus* redrawn from Gabuniya and Kurbatov (1982); **D**, *Megalosauropus broomensis* redrawn from Salisbury et al. (2016); **E**, *Eubrontes giganteus* redrawn from Olsen et al. (1998); **F**, *Jurabrontes curtedulensis* redrawn from Marty et al. (2018); **G**, *Jurabrontes melphiticus* redrawn from Antonelli et al. (2023); **H**, *Iberosauripus grandis* redrawn from Cobos et al. (2014); **I**, *Asianopodus wangi* redrawn from Xing et al. (2021); **J**, *Asianopodus pulvinicalx* redrawn from Matsukawa et al. (2005); **K**, *Asianopodus robustus* redrawn from J. J. Li et al. (2011); **L**, *Asianopodus niui* redrawn from Y. Li et al. (2020); **M**, *Chongqingpus nananensis* redrawn from Foster et al. (2024); **N**, *K. hopii*, redrawn from Lockley et al. (2011); **O**, *Grallator parallelus* redrawn from Olsen et al. (1998). All track outlines are scaled to the same scale. Scale bar equals 10 cm.

Geometric Morphometrics

This analysis tested the affinities of the PGN02 tracks with *M. transjuranicus* and other key theropod ichnotaxa (Fig. 5). Ichnotaxa were selected based on morphological similarity (*M. transjuranicus*, *M. uzbekistanicus*, *A. wangi*, *Asianopodus pulvinicalx*, *Asianopodus niui*, and *Asianopodus robustus*), representative Jurassic theropod ichnotaxa (*Eubrontes giganteus*, *J. curtedulensis*, *Jurabrontes melphiticus*, and *Iberosauripus grandis*), and morphologically different outliers (*Grallator parallelus*, *Chongqingpus nananensis*, *Kayentapus hopii*, and *Eutynichnium lusitanicum*). Landmarks were placed with ImageJ Fiji (v. 1.54; Schindelin et al., 2012). Two different configurations were tested for landmark placement: (i) 6-landmark configuration

TABLE 2. List of the 79 tracks used for geometric morphometrics. The IDs (1–79) are reported. **Abbreviations**: **1CB**, El Castellar site, Teruel, Spain; **BSY**, Bois de Sylleux, Porrentruy, Switzerland; **CP**, Los Corrales del Pelejon, Teruel Province, Spain; **DEIO**, Demnat Iouaridane, Demnat, Morocco; **HA**, Hojapil-Ata, Koitendag National Park, Turkmenistan; **LS**, Lishi site, Hebei Province, China; **PGN**, Plagne tracksite, Plagne France; **SCR**, Sur Combe Ronde, Porrentruy, Switzerland; **SL**, San Leonardo Quarry, Molfetta, Italy; **TCH**, Tchafouè, Porrentruy, Switzerland; **VMX**, Vale de Meios, Pé da Pedreira, Portugal.

ID	Track	Ichnotaxa
1	PGN02-R1	PGN02
2	PGN02-L2	PGN02
3	PGN02-R2	PGN02
4	PGN02-L3	PGN02
5	PGN02-R3	PGN02
6	PGN02-L4	PGN02
7	PGN02-R4	PGN02
8	PGN02-L5	PGN02
9	PGN02-R5	PGN02
10	PGN02-L6	PGN02
11	TCH1030-T6-L1	*Megalosauripus transjuranicus*
12	TCH1030-T7-L2	*Megalosauripus transjuranicus*
13	BSY1040-T1-R1	*Megalosauripus transjuranicus*
14	TCH1030-T2-R2	*Megalosauripus transjuranicus*
15	TCH1030-T2-L3	*Megalosauripus transjuranicus*
16	Lockley et al. (1998:fig. 8)	*Megalosauripus uzbekistanicus*
17	HA-8A	*Megalosauripus uzbekistanicus*
18	HA-8C	*Megalosauripus uzbekistanicus*
19	HA-3A	*Megalosauripus uzbekistanicus*
20	HA-3B	*Megalosauripus uzbekistanicus*
21	HA-3C	*Megalosauripus uzbekistanicus*
22	CP1.1	*Megalosauripus* cf. *transjuranicus*
23	CP1.4	*Megalosauripus* cf. *transjuranicus*
24	CP2.2	*Megalosauripus* cf. *transjuranicus*
25	CP2.4	*Megalosauripus* cf. *transjuranicus*
26	CP3.3	*Megalosauripus* cf. *transjuranicus*
27	CP3.7	*Megalosauripus* cf. *transjuranicus*
28	CP5.1	*Megalosauripus* cf. *transjuranicus*
29	CP5.3	*Megalosauripus* cf. *transjuranicus*
36	SHN.(JJS).ICNO.001E	*Megalosauripus* cf. *transjuranicus*
37	SHN.(JJS).ICNO.001F	*Megalosauripus* cf. *transjuranicus*
38	SHN.(JJS).ICNO.119	*Megalosauripus* cf. *transjuranicus*
39	DEIO XLII	*Megalosauripus* cf. *transjuranicus*
30	VMX.2	*Megalosauripus* sp.
31	VMX.1	*Megalosauripus* sp.
32	Razzolini et al. (2016:fig. 6D)	*Megalosauripus* sp.
33	Razzolini et al. (2016:fig. 6H)	*Megalosauripus* sp.
35	CU-MWC 188.25	*Megalosauripus* sp.
35	Lockley, Meyer, & dos Santos (1998: fig. 8)	*Megalosauripus* sp.
41	ML1875	*Megalosauripus* sp.
42	WAM66.2.51	*Megalosauropus broomensis*
43	WAM64.6.5	*Megalosauropus broomensis*
44	WAM64.6.10	*Megalosauropus broomensis*
45	SCR1500-T1-L8	*Jurabrontes curtedulensis*
46	SCR1500-T1-R7	*Jurabrontes curtedulensis*
47	SCR1500-T1-L7	*Jurabrontes curtedulensis*
48	BSY1050-TR2-R3	*Jurabrontes curtedulensis*
40	DEIO CXXVII/16	*Jurabrontes curtedulensis*
49	SL1-1	*Jurabrontes melphiticus*
50	SL1-2	*Jurabrontes melphiticus*
51	SL1-3	*Jurabrontes melphiticus*
52	SL4b-1	*Jurabrontes melphiticus*
53	SL6-2	*Jurabrontes melphiticus*
54	ACM-ICH 15/3	*Eubrontes giganteus*
55	SGDS 9	*Eubrontes giganteus*
56	AC 45/8	*Eubrontes giganteus*
57	AC 45/1	*Eubrontes giganteus*
58	1CB1.5	*Iberosauripus grandis*
59	MNS96/28	*Iberosauripus grandis*
60	MNS2003/92/14	*Iberosauripus grandis*
61	LS-T6-R3	*Asianopodus wangi*
62	LS-T15-R4	*Asianopodus wangi*
63	LS-T9-R3	*Asianopodus wangi*
64	LS-T4-L2	*Asianopodus wangi*
65	LS-T4-R2	*Asianopodus wangi*
66	LS-T15-L2	*Asianopodus wangi*
67	LS-T15-R3	*Asianopodus wangi*
68	TGU SE-DT1004	*Asianopodus pulvinicalx*
69	IVPP CV 26286.1	*Asianopodus niui*
70	IVPP CV 26286.2	*Asianopodus niui*
71	IVPP CV 26286.3	*Asianopodus niui*
72	Lucas et al. (2024:fig. 7.6 K)	*Asianopodus robustus*
73	UCMP 83668	*Kayentapus hopii*
74	Olsen et al. (1998:fig. 11)	*Grallator parallelus*
75	Olsen et al. (1998:fig. 11)	*Grallator parallelus*
76	Olsen et al. (1998:fig. 11)	*Grallator parallelus*
77	Olsen et al. (1998:fig. 11)	*Grallator parallelus*
78	V1401 (CFNY 1)	*Chongqingpus nananensis*
79	MNHN-MG-P261	*Eutynichnium lusitanicum*

(6-L) and (ii) the 12-landmark configuration (12-L). The same dataset (Table 2) and the R script were used for both landmark configurations. In the 6-landmark configuration, landmarks are defined as follows: landmark 1, tip of the impression of digit IV; landmark 2, tip of the impression of digit III; landmark 3, tip of the impression of digit II; landmark 4, posterior end of the track; landmark 5, posterior ends of the impression of digit II; landmark 6, posterior end of the impression of digit III. In the 12-landmark configuration, the width of the digital impressions was also taken into account. Landmarks 1–6 are placed as previously, while landmarks 7 and 8, 9 and 10, 11 and 12, represented the width of the impressions of digits II, III, and IV, respectively (Fig. 4).

Geometric morphometric analyses were performed in R (v. 4.5.0; R Core Team, 2023) using the Morpho (Schlager, 2017) and Geomorph (Adams & Otárola-Castillo, 2013) packages. Shape alignment was carried out using the ProcSym function in Morpho (Schlager, 2017) which applies a Generalized Procrustes Analysis (GPA) to rotate, translate, and scale specimens in order to minimize the sum of squared distances between corresponding landmarks. Following the alignment, a Principal Component Analysis (PCA) was conducted to explore morphological variation within the morphospace. To fully investigate track variability, four hypothetical morphologies were generated by projecting the mean GPA landmark configuration to ± 2 standard

deviations (SD) along the first two principal component axes. This highlights the extreme configurations of the morphospace, representing the most divergent shapes statistically predicted. To evaluate the influence of ichnotaxonomic attribution on footprint shape, Procrustes Analysis of Variance (Procusters ANOVA) was performed using residual randomization permutation procedures (RRPP) with 1,000 permutations. This analysis was conducted on both the 6-landmark and 12-landmark datasets. To assess potential allometric effects on shape variation, we plotted PC1 against the logarithm of the centroid size (logCS) after the implementation of a Spearman's rank correlation analysis.

Institutional Abbreviations—**AC** or **ACM-ICH**, Appleton Cabinet, Beneski Museum of Natural History, Amherst, USA; **CUBG**, China University of Geosciences, Beijing, China; **CU-MWC**, University of Colorado Denver-Museum of Western Colorado, Boulder, USA; **DinoPlagne**, DinoPlagne Terre Valserhône, Plagne, France; **DST**, Dipartimento di Scienze della Terra, Firenze, Italy; **EAVP**, European Association of Vertebrate Paleontologists, Karlsruhe, Germany; **IVPP CV**, Institute of Vertebrate Paleontology and Paleoanthropology, Beijing, China; **MGGC**, Collezione di Geologia, Museo Giovanni Capellini, Bologna, Italy; **MICIU**, Ministerio de Ciencia, Innovación y Universidades, Madrid, Spain; **ML**, Museu de Lourinhã, Lourinhã, Portugal; **MNHN-MG**, Museu Nacional de História Natural da Universidade de Lisboa, Lisboa, Portugal; **MSN**, Museo Numantino de Soria, Soria, Spain; **PPC**, Professional Palaeontological Consulting, Basel, Switzerland; **SGDS**, St. George Dinosaur Discovery Site at Johnson Farm, St. George, USA; **SHN.(JJS).ICNO**, Sociedade de História Natural, Torres Vedras, Portugal; **SNSF**, Swiss National Science Foundation, Bern, Switzerland; **TGU**, Tokyu Gakugei University, Tokyo, Japan; **UCMP**, University of California Museum of Paleontology, Berkeley, USA; **V1401 (CFNY 1)**, Chongqing Museum of Natural History, Chongqing, China; **WAM**, Western Australian Museum, Perth, Australia.

Anatomical Abbreviations—**II ^ III**, digit II–digit III interdigital angle; **II ^ IV**, digit II–digit IV interdigital angle; **III ^ IV**, digit III–digit IV interdigital angle; **AT**, anterior triangle; **AT l/FW**, mesaxony; **dII**, digit II length; **dIII**, digit III length; **dIV**, digit IV length; **FL**, footprint length; **FW**, footprint width; **FL/FW**, footprint length to footprint width ratio; **h**, hip height; **P**, pace; **S**, stride; **te**, digit III projection; **wII**, digit II width; **wIII**, digit III width; **wIV**, digit IV width.

RESULTS

Morphological Comparison Results

The PGN02 tracks are large tridactyl asymmetric footprints, longer than wide, that display well-defined margins, with digital pad impressions and claw traces. Track fidelity is high and the morphological preservation grade is 3, the maximum on the scale of Marchetti et al. (2019), despite the lack of skin/scale impressions. The FL ranges from 30–33 cm ('large'; Marty et al., 2018), while footprint width ranges from 16.5–18.5 cm (mean FL: 31.6 cm; and FW: 17.6 cm). The pad impression formula is 2-3-4 (for digits II, III, and IV, respectively). The impression of the fourth pad has a rounded shape and is the widest of all the phalangeal pad impressions. It forms the rounded heel of the track and is not aligned with the impression of digit III (Figs. 5, 6). The interdigital angles are low, varying from 19–27° for II ^ III, 16–26° for III ^ IV, and 35–52° for II ^ IV (mean II ^ III: 25°, mean III ^ IV: 24° and mean II ^ IV: 49°). Mesaxony (AT l/FW) is highly variable, ranging from 0.49–0.88 (mean value of 0.7). Regarding the trackway parameters, stride ranges from 109–113 cm (mean S: 111 cm) and pace length ranges from 218–222 cm (mean P: 220 cm). Trackmaker speed is estimated as 6.3 km/h, and trackway direction is 29°N. All measurements are in Table 1.

Whole-Track Analysis Results

The comparison of the PGN02 tracks with the holotype of *M. transjuranicus* (TCH1030-T6-L1; Fig. 6) shows strong affinities in overall morphology, pad impression configuration, and claw traces in the impression of digit III. Of the 10 analyzed tracks six of them (PGN02-R1, PGN02-R2, PGN02-R5, PGN02-L2, PGN02-L3, and PGN02-L6), show a strong and nearly complete morphological overlap. In contrast, the remaining four tracks (PGN02-R3, PGN02-R4, PGN02-L4, and PGN02-L5), show differences in the position of digit II impressions being more internal and closer to digit III impression and thus resulting in lower interdigital angles (II ^ III and II ^ IV). Across all PGN02 tracks, the position of the impressions of the phalangeal pads consistently aligns and overlaps with those of TCH1030-T6-L1, with the fourth and last phalangeal pad impressions of digit IV having the best overlap with the corresponding pad impression of TCH1030-T6-L1.

Comparison of PGN02 tracks with the holotype of *A. wangi* (LS-T6-R3; Fig. 7) shows strong morphological affinities in both shape and pads impression configuration. In two of the tracks (PGN02-R1 and PGN02-R3) the overlap is almost complete. However, the remaining tracks (PGN01-R2, PGN02-R4, PGN02-R5, PGN02-L2, PGN02-L5, and PGN02-L6), show discrepancies in the position of the impression of the fourth pad of digit IV being asymmetrically positioned relative to the impression of digit III for PGN02 tracks, which contrasts with the aligned and symmetrical placement seen in *A. wangi* (Xing et al., 2021).

Geometric Morphometric Results

Two landmark configurations (6 and 12 landmarks) were placed as shown in Fig. 4. Principal Component Analyses were performed for each configuration (Figs. 8, 9), with shape variations at ± 2 SD. In both analyses, PC1 represents footprint width, whereas PC2 represents the distance between the posterior end of the footprint and the posterior end of the impression of digit II (distance between landmarks 4 and 5, see mean shapes in Figs. 8, 9).

In the 6-landmark configuration (Fig. 8), PC1 and PC2 explain 64.82% of the total variance. Higher PC1 scores correspond to footprints showing higher divarication angles while higher PC2 scores indicate specimens with a greater distance between the posterior end of the footprint and the posterior end of the impression of digit II. The resulting morphospace is characterized by partial overlap in the positive quadrants but also features several ichnotaxa located in the negative space (such as *M. transjuranicus* and *G. parallelus*), areas in which many taxa show limited or no overlap. Tracks assigned to *Megalosauripus* primarily cluster within the positive PC2 morphospace. Specifically, the PGN02 specimens plot in close proximity to *M. transjuranicus* within the negative PC1/positive PC2 quadrant. This position clearly distinguishes PGN02 from *M. uzbekistanicus*, which occupies a distinct region in the positive PC1 quadrant. While the distribution of *Asianopodus* is notably broader with *A. wangi* extending significantly into the negative PC2 space but being the closest to PGN02 and *M. transjuranicus*. PGN02 in fact exhibits the greatest affinity with *A. wangi* specimens among the different *Asianopodus* ichnotaxa. The large theropod ichnotaxa *Jurabrontes* and *Iberosauripus* are characterized by high PC1 values, indicating high divarication angles in these tracks. Conversely, *G. parallelus* occupies the negative PC1–PC2 quadrant, characterized by low divarication angles and short distance between the posterior

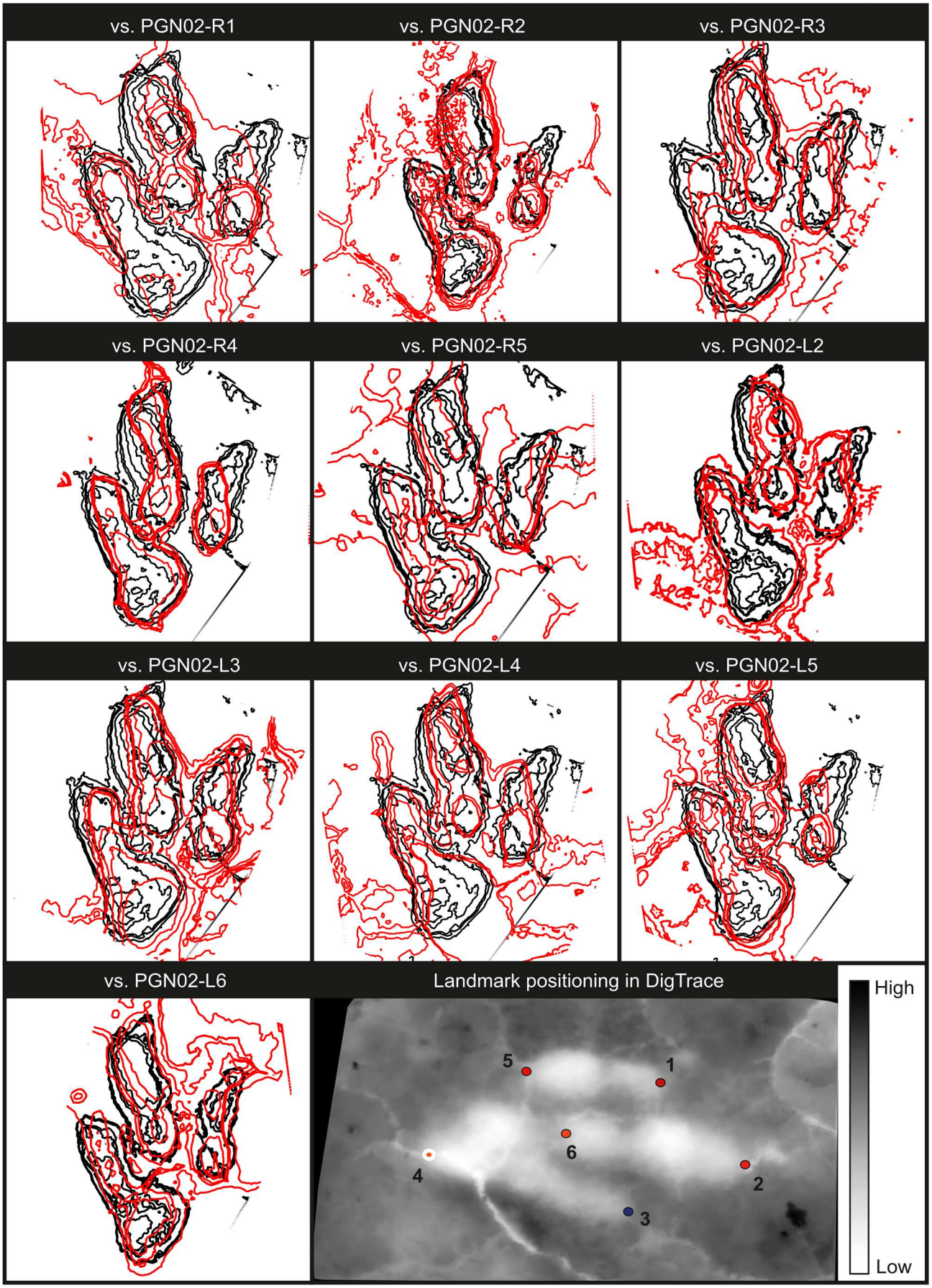


FIGURE 6. Whole-Track Analysis of the Plagne tracks with the holotype of *Megalosauripus transjuranicus* performed in DigTrace.

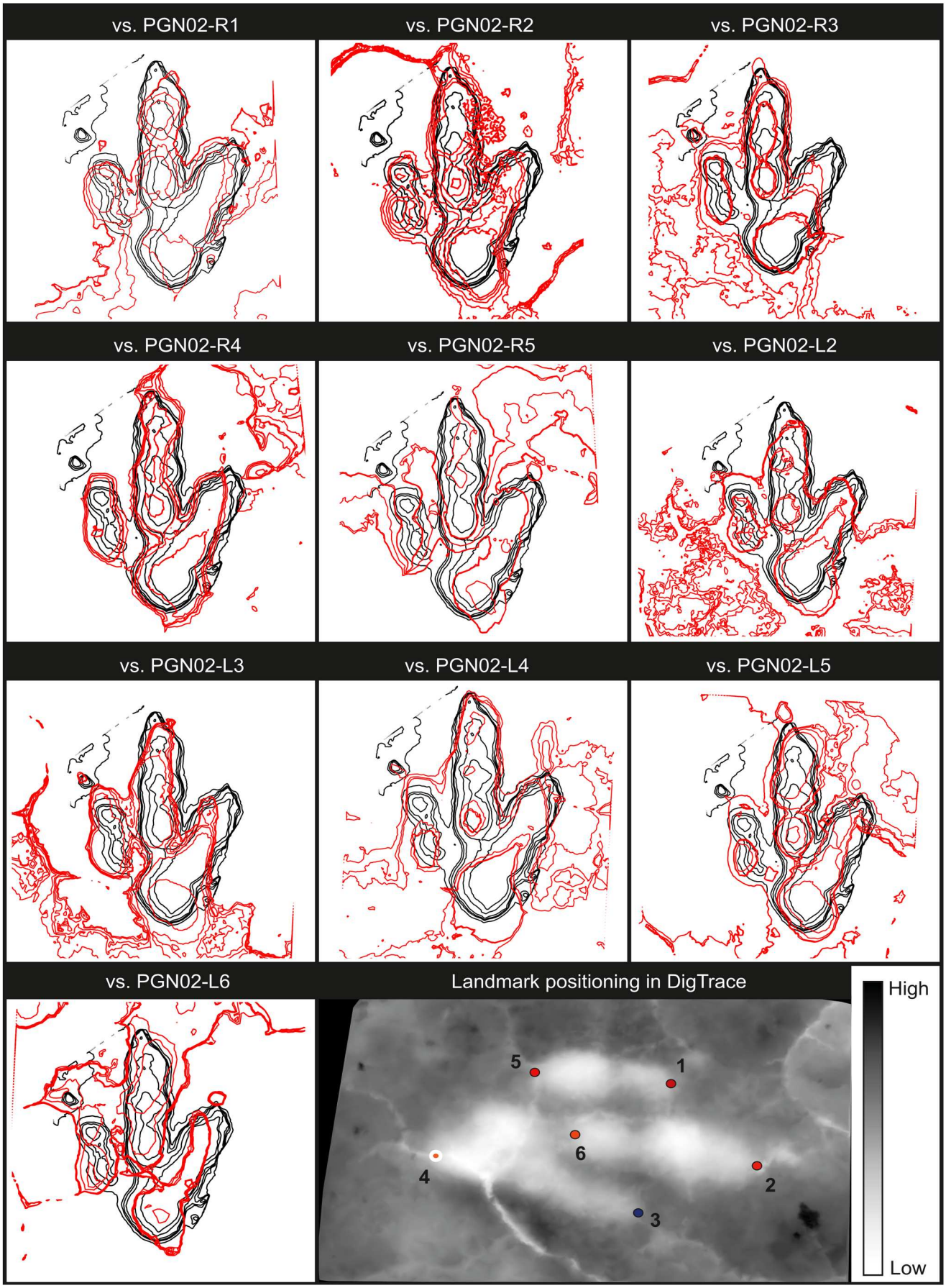


FIGURE 7. Whole-Track Analysis of the Plagne tracks with the holotype of *Asianopodus wangi* performed in DigTrace.

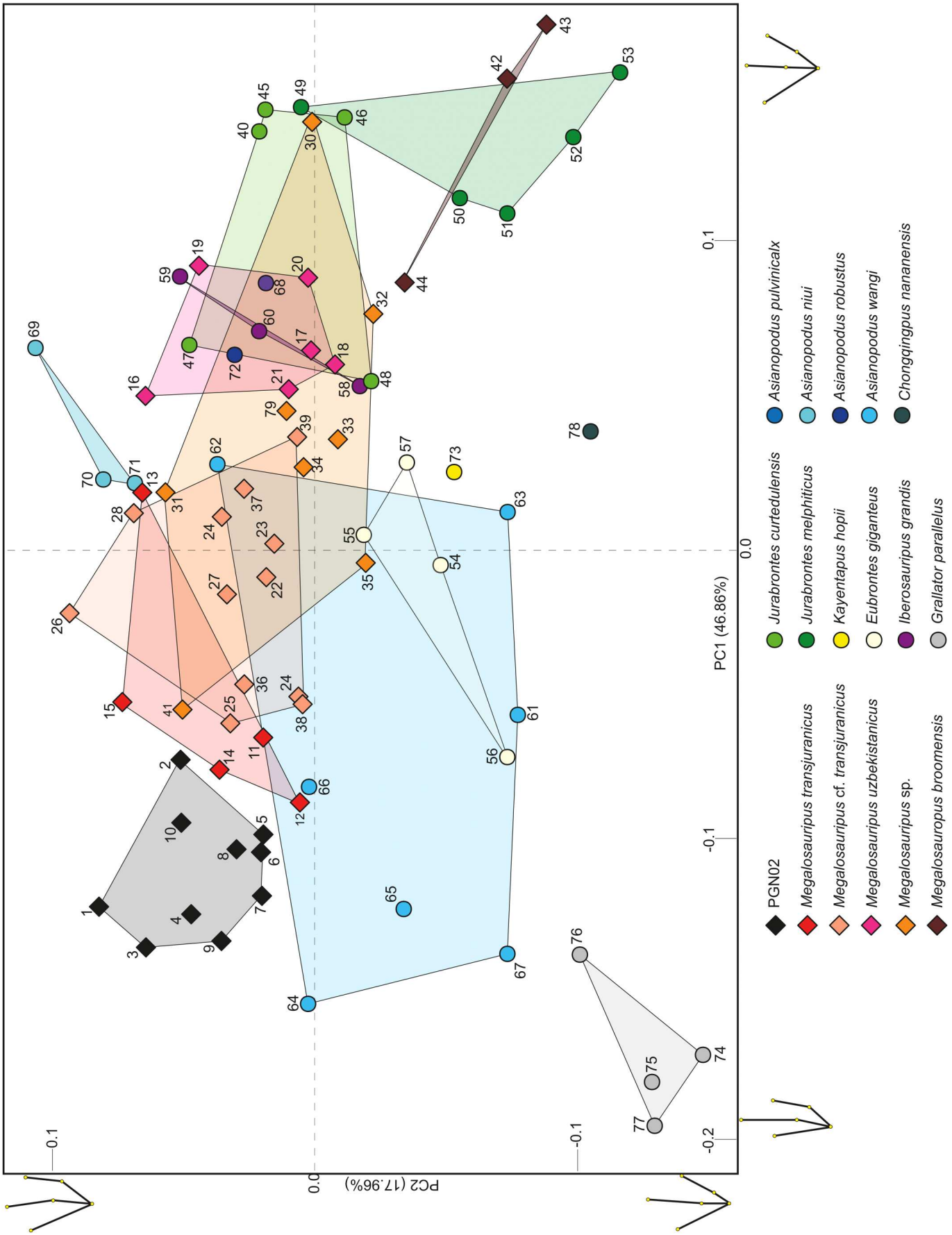


FIGURE 8. Principal Component Analysis of the Plagne tracks and other theropod ichnotaxa using the 6-landmarks configuration. Individual tracks are grouped according to previously published ichnotaxonomic assignments. See Table 2 for which track the ID refers to.

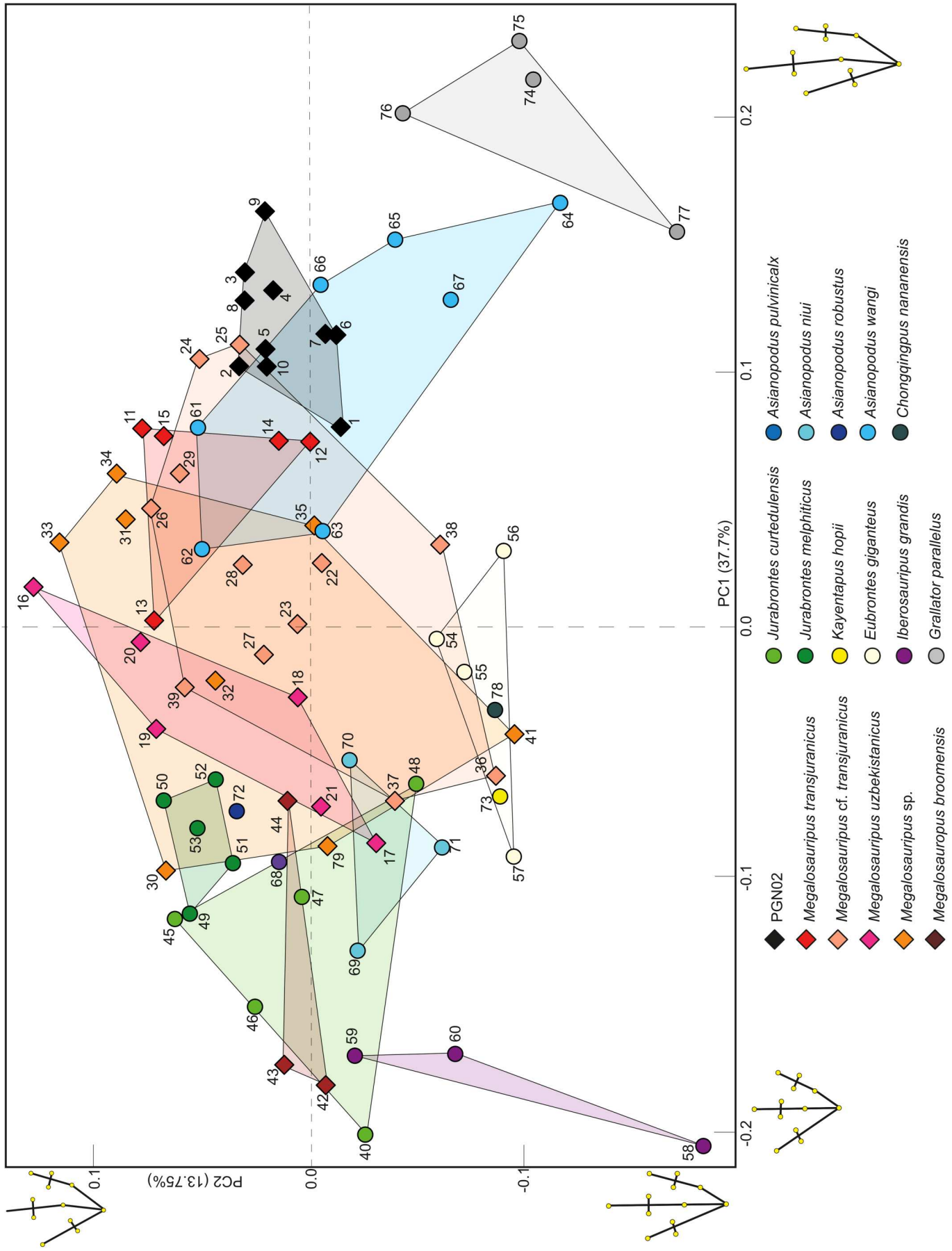


FIGURE 9. Principal Component Analysis of the Plagne tracks and other theropod ichnotaxa using the 12-landmark configuration. Individual tracks are grouped according to previously published ichnotaxonomic assignments. See Table 2 for which track the ID refers to.

end of the footprint and the posterior end of the impression of digit II. We note that digit III impression protrusion (mesaxony sensu Lockley, 2009) is a secondary influence on the distribution of specimens along PC1, with lower mesaxony related to higher PC1 scores and vice versa. The Spearman's rank test correlation of PC1 scores and the absolute track size indicates a moderately positive correlation ($p = 1.56 \times 10^{-8}$; rho value = 0.5936), that could be consistent with allometry influencing their distribution in the morphospace.

In the 12-landmark configuration (Fig. 9), the total variance explained by PC1 and PC2 is 51.45%. Tracks showing higher divarication have lower PC1 scores, while those with a larger distance between the posterior ends of the footprint and the posterior end of digit II impression plot at lower PC2 scores. The resulting morphospace is broader and more diffuse with increased overlap among ichnotaxa across all quadrants, and no ichnotaxa forming a clearly isolated cluster with the exception of *Grallator*. The *Megalosauripus* tracks remain closely associated with the PGN02 and *A. wangi* tracks, although this combined distribution occupies a large portion of the morphospace and approaches other morphologically distinct ichnotaxa (e.g., *J. melphiticus*). *Asianopodus* tracks overlap with the *Megalosauripus* distribution in the morphospace. The large theropod ichnotaxa *Jurabrontes* and *Iberosauripus* are characterized by relatively low PC1 values, with the *J. melphiticus* forming a tight cluster, whereas *J. curtedulensis* and *I. grandis* occupy a broader region of the morphospace. *Grallator parallelus* plots in the quadrant, characterized by low divarication angles and a short distance between the posterior end of the footprint and the posterior end of the impression of digit II. In this case, mesaxony continues to influence the distribution of specimens along PC1, with lower mesaxony tracks having low PC1 values and vice versa. The Spearman's rank test ($p = 1.72 \times 10^{-9}$; rho value = −0.617) indicates a moderate negative correlation consistent with allometric influences on shape variation.

Procrustes ANOVA for the 6-landmark configuration revealed a significant effect of ichnotaxa on shape variation ($F_{16, 62} = 7.02$; $p < 0.001$), with ichnotaxonomic grouping explaining 64% of the total morphological variance ($R^2 = 0.64$). This indicates that, despite partial overlaps within PCA morphospace, ichnotaxa have distinguishable shapes (indicating they are morphologically distinct). For the 12-landmark configuration, the results were similarly significant ($F_{16, 62} = 5.50$; $p < 0.001$), confirming that the mean shapes of each ichnotaxon remain statistically distinct even with increased landmark density. However, the proportion of variance explained by ichnotaxonomic grouping is lower ($R^2 = 0.587$) compared to the 6-landmark set.

DISCUSSION

Our analysis indicates that the PGN02 tracks exhibit significant morphological and morphometric similarities to both *M. transjuranicus* and *A. wangi*. Geometric morphometric findings position PGN02 within a morphospace that is situated between the two ichnotaxa. To resolve this ambiguity and determine the most appropriate ichnotaxonomic classification for the PGN02 tracks, the following discussion will critically examine the diagnostic features of the PGN02 tracks alongside those of *M. transjuranicus* and *A. wangi*, as well as the Whole-Track Analysis and geometric morphometrics results.

Morphological Comparisons

The PGN02 tracks share overall similar parameters when compared with *M. transjuranicus*. The main differences are given by FL (ranging from 30–33 cm for PGN02 and from 35.5–44.5 cm for *M. transjuranicus*), divarication angles (ca. 10° less for both II ^ III and III ^ IV in PGN02 tracks), and S (ranging from 218–222 cm for PGN02 and from 235–301 cm for *M. transjuranicus*). The PGN02 tracks are smaller and narrower than *M. transjuranicus*; however, they share a similar FL/FW ratio (mean FL/FW: 1.8 for PGN02 and 1.5 for *M. transjuranicus*), moderate mesaxony (AT l/FW ranges from 0.48–0.87 in PGN02 and 0.35–0.73 in *M. transjuranicus*), pad impression formula, and the impression of the fourth pad of digit IV, which is proportionally and morphologically similar (rounded and the widest one), serves as the 'heel' impression and posterior end of the track. The visible morphological differences in the PGN02 tracks (lower FL, lower interdigital impression angles, shorter stride length) compared to *M. transjuranicus* can be explained by a smaller Plagne trackmaker, as tracks generally increase in size and width in relation to the body size and presumed greater ontogenetic stage of the trackmaker (Lallensack et al., 2020). Consequently, if *M. transjuranicus* corresponds to a larger individual trackmaker, it is expected to have a longer FL, more divergent digits, and a greater stride length (Davidson et al., 2025; Enriquez et al., 2020; Lallensack et al., 2020).

Whole-Track Analysis Discussion

The comparison of the PGN02 tracks with the holotype of *M. transjuranicus* reveals that the outline morphology and position of the phalangeal pad impressions, particularly for the impression of the fourth pad of digit IV, consistently match those of the *M. transjuranicus* holotype (Fig. 6).

The main difference lies in the shape of the impression of digit II, which is narrower in the PGN02 tracks than in TCH1030-T6-L1. This is particularly evident in PGN02-L4, PGN02-L5, PGN02-R2, and PGN02-R4. In PGN02-R4, a further difference is in shape of the impression of digit III. It is narrower only in the central part (2nd phalangeal pad impression) and is wider, as in all the other tracks of the trackway, at both posterior and anterior ends. This difference in digital impression width, given its morphology, is interpreted as related to sediment collapse and deformation during the registration of the tracks and is explainable by a local difference in substrate properties.

The comparison of the PGN02 tracks with the *A. wangi* holotype reveals that the outline morphology and shape of the phalangeal pad impressions largely overlap, however the position of the impression of the fourth pad of digit IV differs significantly (Fig. 7). These are key diagnostic features of both *M. transjuranicus* and *A. wangi*. In *A. wangi*, the impression of the fourth pad of digit IV is symmetrically aligned with the impression of digit III (Xing et al., 2021), whereas in *M. transjuranicus*, it is asymmetrically positioned relative to the impression of digit III (Razzolini et al., 2017). Although the PGN02 tracks exhibit strong overlap and morphological compatibility with both ichnotaxa, the asymmetrical position and configuration of this pad impression relative to the impression of digit III matches closely with *M. transjuranicus*, supporting attribution to this ichnotaxon.

Geometric Morphometric Discussion

The GM results of this study show that shape variation among large theropod ichnotaxa is sensitive to landmark configuration. Principal Component Analyses based on 6- or 12-landmarks exhibit different outcomes (Figs. 8, 9), despite using the same dataset (Table 2). In the 6-landmark configuration (Fig. 8), the ichnotaxa we considered are more clearly separated than in the 12-landmark configuration (Fig. 9). This reflects the proportion of total variance captured by the first two principal components, which for the 6-landmark configuration is 64.82% (see Fig. 4A) versus 51.45% for the 12-landmark configuration (cumulative variance difference = 13.37%). In the 12-landmark configuration,

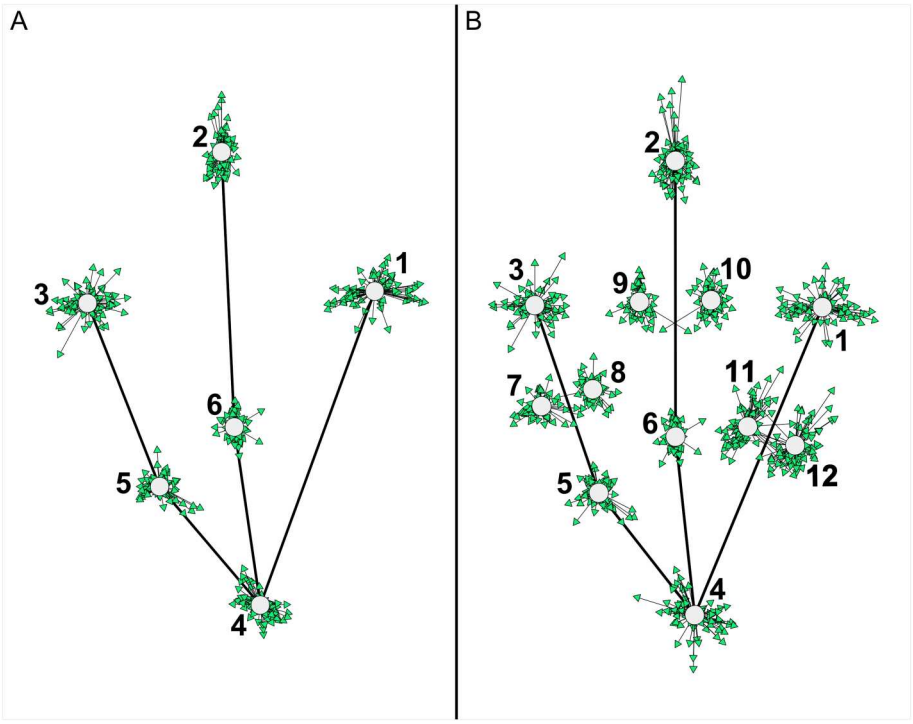


FIGURE 10. **A**, landmark displacement plot for the 6-landmark configuration; **B**, landmark displacement plot for the 12-landmark configuration.

this indicates a redistribution of shape variance across a greater number of dimensions rather than a loss of the ichnotaxonomic signal. As noted by Lallensack et al. (2020), an increase in the number of landmarks can result in less clear or more complex PCA results by capturing more detailed (finer scale) aspects of footprint shape. This is especially relevant when some landmarks are more prone to measurement error and/or are less functionally relevant (Lallensack et al., 2020). Landmarks corresponding to the width of the impression of digit IV (landmarks 11 and 12, Fig. 4) are usually the most variable (Fig. 10) due to the fact that some ichnotaxa (e.g., *M. transjuranicus*, *A. wangi*, *J. curtedulensis*, or *J. melphiticus*; Fig. 5) have a digit IV impression that corresponds with the posterior end of the footprint, while other ichnotaxa (e.g., *E. giganteus*, *A. robustus*, *A. pulvinicalx*, or *A. niui*; Fig. 5) have a digit IV impression that ends before the posterior margin of the footprint. Other digital impressions are usually more conservative across all ichnotaxa, and consequently the landmarks associated with their width (landmarks 7–8 and 9–10) show less variability, at least along FL, while expressing more variability along FW (Fig. 10).

The broader and more clustered morphospace obtained with the 12-landmark configuration (Fig. 9) may reflect the increased shape variability associated with digital impression width information, a parameter more strongly influenced by preservational, functional, or substrate-related effects than other track parameters. Since the application of GM to theropod tracks is meant to help in track classification (e.g., Abrahams et al., 2021; Castanera et al., 2015), the use of landmarks that have lower ichnotaxonomic relevance, such as the digital impression width, should be avoided to prevent introducing variability to potential ichnotaxonomic signals. Instead, the use of 6-landmarks, associated with the major characteristics of tracks (i.e., FL, FW, and divarication angles) proves to be a more meaningful and efficient option for capturing the ichnotaxonomic variation in theropod tracks as it has lower landmark displacement (Fig. 10) and clearer differentiations in the PCA morphospace (Fig. 8). While both landmark configurations reveal statistically significant differences between ichnotaxa, the 6-landmark configuration attributes a greater proportion of variance to ichnotaxonomic grouping ($F = 7.02$; $R^2 = 0.64$) compared to the 12-landmark configuration ($F = 5.50$; $R^2 = 0.59$). In general, these results highlight the need to evaluate landmark selection and number in dinosaur ichnology.

Ichnotaxonomic Interpretation of Geometric Morphometrics

The application of GM to a wide range of theropod ichnotaxa provides insights into the overall ichnotaxonomic interpretation and complements our other methodologies (i.e., qualitative, WTA). Figure 8 shows that the smaller and more gracile ichnogenus *Grallator* is differentiated from *Megalosauripus* and the other larger ichnotaxa. Among the large and giant theropod ichnotaxa (*Eubrontes*, *Jurabrontes*, *Iberosauripus*, and *Chongqingpus*), distinct shape differences are also evident, separating them from *Megalosauripus.* Interestingly, *Megalosauripus* and *Megalosauropus* tracks are well separated, supporting the hypothesis of Razzolini et al. (2017) that these ichnogenera are not synonyms (also see Foster et al., 2024; Lockley, Meyer, & dos Santos, 1996, 1998; Salisbury et al., 2016; Thulborn, 2001). The distribution of ichnotaxa in both 6-landmarks and 12-landmarks PCAs (Figs. 8, 9) further shows allometric effects identified by the Spearman's rank test, with more gracile morphotypes (e.g., PGN02 tracks, *G. parallelus*, and *A. wangi*) occupying different morphospace regions than more robust morphotypes (e.g., *J. curtedulensis*, *J. melphiticus*, and *I. grandis*).

The PGN02 tracks occupy a region of the morphospace that, in both landmark configurations, lies between *M. transjuranicus* and *A. wangi*, and indicates that, based on GM results alone, PGN02 tracks do not morphometrically fit within one single ichnotaxon. In both configurations (Figs. 8, 9), *A. wangi* occupies a

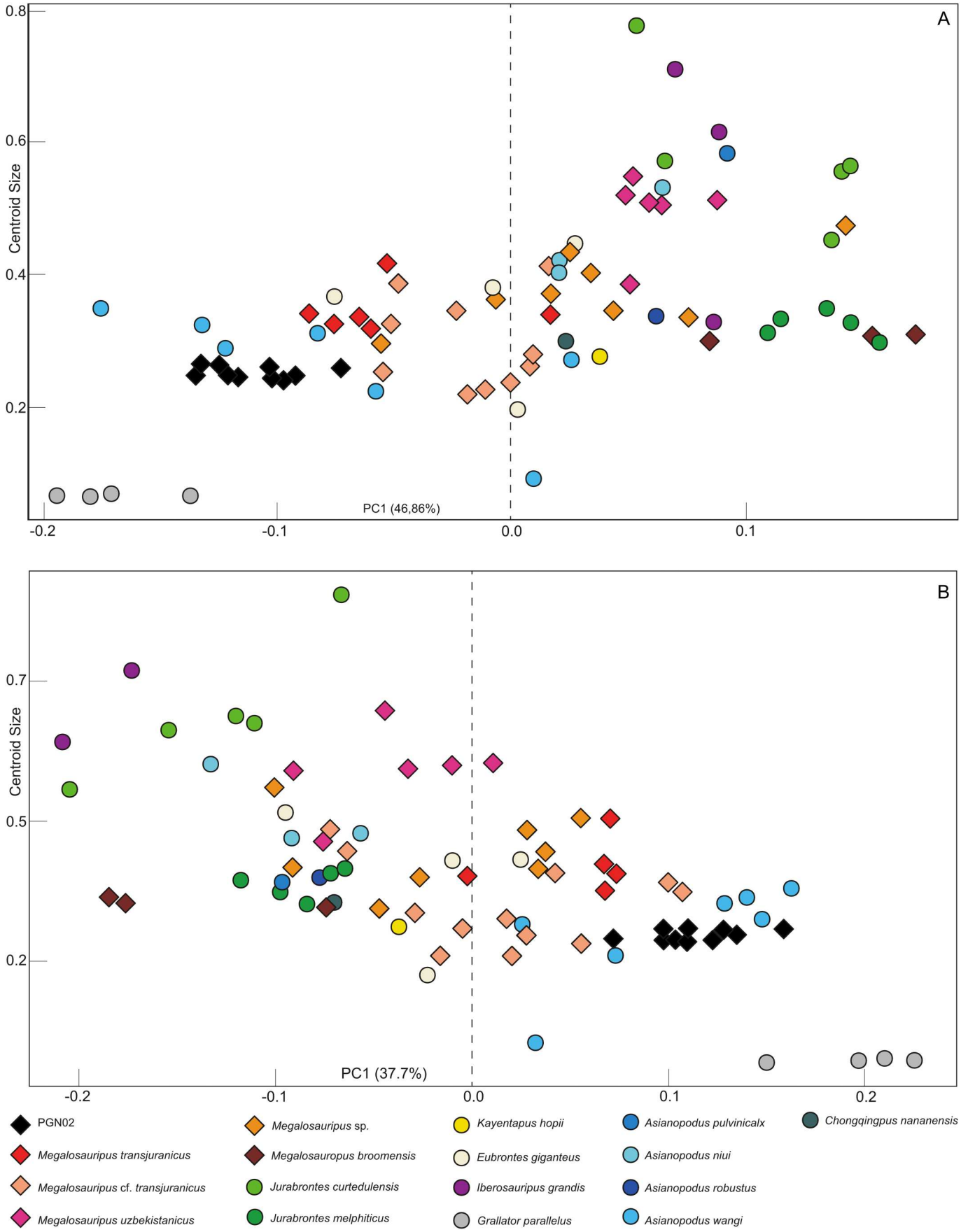


FIGURE 11. **A**, plot of PC1 versus centroid size from the 6-landmark configuration PCA; **B**, plot of PC1 vs. centroid size for the 12-landmark configuration.

broader morphospace distribution, whereas PGN02 and *M. transjuranicus* form more constrained groupings. Despite *M. transjuranicus* tracks consistently plotting close to PGN02, the two do not overlap perfectly. PGN02 tracks actually overlap more with *A. wangi* in the 12-landmark configuration (Fig. 9). This may be partly explained by relatively wider digital impressions associated with tracks assigned to *M. transjuranicus*. However, they share a fundamentally similar overall morphology that is supported by the WTA analysis (Fig. 6). Moreover, the centroid size vs. PC1 plot (Fig. 11) shows a shift of *M. transjuranicus* specimens towards larger centroid sizes and supports the hypothesis that the PGN02 tracks were made by a smaller trackmaker characterized by lower FL and narrower interdigital angles (validated by the rho values of the Spearman's tests; see Morphological discussion). It also raises the possibility of ontogenetic factors on track morphology, as discussed by Lallensack et al. (2020).

Altogether, the attribution of PGN02 to *M. transjuranicus* is supported by linear measurements (see Morphological Comparison results), WTA (see Whole-Track Analysis results) and the GM results. When comparing PGN02 to *A. wangi*, linear measurements in Xing et al. (2021) show similar dimensions, but a significant morphological difference lies in the asymmetrical position of the impression of the fourth pad of digit IV (visible in the PGN02 tracks). The asymmetrical/symmetrical position of this pad impression is used to distinguish these two ichnotaxa (Xing et al., 2021), and with respect to this character, PGN02 tracks align more closely with *M. transjuranicus* than with *A. wangi* (Figs. 6, 7).

Paleogeographic and temporal distributions further support the assignment of PGN02 to *M. transjuranicus*, which is based on tracks known from the Upper Jurassic (Oxfordian–Tithonian) of Switzerland, Spain, Portugal, and Morocco (Belvedere et al., 2019; Castanera et al., 2021; Castanera et al., 2023; Razzolini et al., 2017). Conversely, tracks assigned to *A. wangi* are only found in the Lower Cretaceous of China (Berrasian; Xing et al., 2021). Given this geographic and temporal separation, an assignment of the PGN02 tracks to *M. transjuranicus* is the most parsimonious interpretation. Nevertheless, the morphological similarities between *M. transjuranicus* and *A. wangi* suggest that their relationship should be further explored (Castanera et al., 2023; Foster et al., 2024; Xing et al., 2021).

Megalosauripus cf. *transjuranicus* (Figs. 8, 9; ID 22–29 in Table 2) tracks, from the Lower Cretaceous (Berriasian) Los Corrales del Pelejón tracksite of Spain (Castanera et al., 2023), also plot close to *M. transjuranicus* in the morphospace. Morphological similarity between these tracks, *M. transjuranicus* and other theropod ichnotaxa has been discussed by Castanera et al. (2023). Although the PCA results presented here, together with previously reported morphological affinities (Castanera et al., 2023), support a close relationship between these two track types, further analyses are required to fully resolve the ichnotaxonomic status of these tracks relative to *M. transjuranicus*.

CONCLUSION

The qualitative and quantitative analysis of the PGN02 theropod tracks from the Plagne tracksite (French Jura) leads to the following conclusions:

- The Plagne theropod tracks are best referred to *M. transjuranicus*. This attribution is supported by an integrated assessment using morphological characteristics, track and trackway parameters, WTA and GM results. Although the GM results alone do not definitively identify the tracks, they consistently indicate a close morphological relationship with *M. transjuranicus*, in conjunction with our other lines of evidence;
- The PGN02 trackmaker was morphologically similar to the trackmaker producing *M. transjuranicus* but smaller in size (mean FL is 31.6 cm for PGN02 and 42.5 cm for *M. transjuranicus*). This is supported by allometric patterns observed in the GM analyses suggesting size-related shape variation;
- The Plagne tracks extend the known paleogeographic distribution of *M. transjuranicus*;
- The close morphological and morphometric relationship observed between *M. transjuranicus* and *A. wangi* calls for further comparative research.

ACKNOWLEDGMENTS

We sincerely thank DinoPlagne and its staff for allowing us to work at the tracksite. P. Landry for the support during the fieldwork; L. Xing (CUGB) and H. Yin (CUGB) for sharing the 3D model of *A. wangi* holotype; and M. Contessi (MGGC) for the 3D models of *M. uzbekistanicus*. We also thank the anonymous reviewers for their helpful comments that improved the quality and overall clarity of the manuscript. We appreciate the handling editor, S. Salisbury, for his suggestions and manuscript processing. VG was funded by EAVP ERG 2024. MB was funded by the DST 'Internationalisation Grants.' DC is supported by a Ramón y Cajal fellowship (RYC2023-044333-I) funded by MICIU/AEI 935 /10.13039/501100011033 and FSE+. LS acknowledges support from the SNSF grant (200021_192036). CM is supported by PPC. This work is a contribution to the e-Col + project funded by the Programme d'Investissements d'Avenir (ANR 21 ESRE 0053).

AUTHOR CONTRIBUTIONS

CRediT: VG: Conceptualization, Data curation, Investigation, Writing – original draft, Writing – review & editing; LS: Conceptualization, Formal analysis, Funding acquisition, Supervision, Writing – review & editing; CAM: Conceptualization, Supervision, Writing – review & editing; AR: Formal analysis, Investigation, Writing – review & editing; DC: Writing – review & editing; EF: Conceptualization, Investigation, Writing – review & editing; JDM: Writing – review & editing; MB: Conceptualization, Formal analysis, Funding acquisition, Investigation, Supervision, Writing – review & editing.

DATA AVAILABILITY STATEMENT

The high-resolution 3D model of the PGN02 trackway, high-resolution images of each single PGN02 footprint and all the single photos taken to generate the 3D model of the PGN02 trackway are available in the paper and the supplementary online file here: https://doi.org/10.6084/m9.figshare.30720329.v1.

DISCLOSURE STATEMENT

No potential conflict of interest was reported by the author(s).

ORCID

Vincenzo Gesualdi http://orcid.org/0009-0003-0818-1969
Lara Sciscio http://orcid.org/0000-0003-4178-2881
Christian A. Meyer http://orcid.org/0000-0002-5069-8924
Alessandro Riga http://orcid.org/0000-0002-7240-0009
Diego Castanera http://orcid.org/0000-0003-3950-1630
Emmanuel Fara http://orcid.org/0000-0002-7991-4467
Jean-David Moreau http://orcid.org/0000-0003-2978-5983
Matteo Belvedere http://orcid.org/0000-0002-0135-4455

LITERATURE CITED

Abrahams, M., Bordy, E. M., & Knoll, F. (2021). Hidden for one hundred years: A diverse theropod ichnoassemblage and cross-sectional tracks from the historic Early Jurassic Tsikoane ichnosite (Clarens Formation, northern Lesotho, southern Africa). *Historical Biology*, *33*(10), 2504–2519. doi:10.1080/08912963.2020.1810681

Adams, D. C., & Otárola-Castillo, E. (2013). Geomorph: An R package for the collection and analysis of geometric morphometric shape data. *Methods in Ecology and Evolution*, *4*(4), 393–399. doi:10.1111/2041-210X.12035

Agisoft, L. L. C. (2024). *Metashape professional edition (Version 2.2.2) [Computer software]*. Agisoft LCC.

Alexander, R. M. (1976). Estimates of speeds of dinosaurs. *Nature*, *261*(5556), 129–130. doi:10.1038/261129a0

Antonelli, M., Petti, F. M., Conti, J., Sacco, E., Petruzzelli, M., Spalluto, L., & Wagensommer, A. (2023). Lower Cretaceous dinosaur footprints from the Molfetta tracksite (Apulia, southern Italy). *Cretaceous Research*, *142*, 105388–25. doi:10.1016/j.cretres.2022.105388

Belvedere, M., Bennett, M. R., Marty, D., Budka, M., Reynolds, S. C., & Bakirov, R. (2018). Stat-tracks and mediotypes: Powerful tools for modern ichnology based on 3D models. *PeerJ*, *6*, e4247–25. doi:10.7717/peerj.4247

Belvedere, M., Castanera, D., Meyer, C. A., Marty, D., Mateus, O., Silva, B. C., Santos, V. F., & Cobos, A. (2019). Late Jurassic globetrotters compared: A closer look at large and giant theropod tracks of North Africa and Europe. *Journal of African Earth Sciences*, *158*, 103547–10. doi:10.1016/j.jafrearsci.2019.103547

Bernier, P. (1984). Les formations carbonatées du Kimméridgien et du Portlandien dans le Jura méridional. Stratigraphie, micropaléontologie, sédimentologie. *Documents des Laboratoires de Géologie de Lyon*, *92*, 3–443.

Budka, M., Bakirov, R., Deng, S., Falkingham, P., Reynolds, S. C., & Bennett, M. R. (2016). *DigTrace Pro (Version 1.0.)*. [Computer Software]. Bournemouth University.

Budka, M., Bakirov, R., Falkingham, P., Reynolds, S. C., Underhill, S., & Bennett, M. R. (2016). *DigTrace Pro: User manual*. Bournemouth University.

Castanera, D., Aurell, M., Canudo, J. I., Cuenca-Bescós, G., Gasca, J. M., & Bádenas, B. (2023). Paleoecology and paleoenvironment of the Early Cretaceous theropod-dominated ichnoassemblage of the Los Corrales del Pelejón tracksite, Teruel Province, Spain. *Palaeogeography, Palaeoclimatology, Palaeoecology*, *630*, 111761–14. doi:10.1016/j.palaeo.2023.111761

Castanera, D., Belvedere, M., Marty, D., Paratte, G., Lapaire-Cattin, M., Lovis, C., & Meyer, C. A. (2018). A walk in the maze: Variation in Late Jurassic tridactyl dinosaur tracks from the Swiss Jura Mountains (NW Switzerland). *PeerJ*, *6*, e4579–33. doi:10.7717/peerj.4579

Castanera, D., Colmenar, J., Sauqué, V., & Canudo, J. I. (2015). Geometric morphometric analysis applied to theropod tracks from the Lower Cretaceous (Berriasian) of Spain. *Palaeontology*, *58*(1), 183–200. doi:10.1111/pala.12132

Castanera, D., Malafaia, E., Silva, B. C., Santos, V. F., & Belvedere, M. (2021). New dinosaur, crocodylomorph and swim tracks from the Late Jurassic of the Lusitanian Basin: Implications for ichnodiversity. *Lethaia*, *54*(2), 260–270. doi:10.1111/let.12402

Cobos, A., Lockley, M. G., Gascó, F., Royo-Torres, R., & Alcalá, L. (2014). Megatheropods as apex predators in the typically Jurassic ecosystems of the Villar del Arzobispo Formation (Iberian Range, Spain). *Palaeogeography, Palaeoclimatology, Palaeoecology*, *399*, 31–41. doi:10.1016/j.palaeo.2014.02.008

Colombié, C., & Strasser, A. (2005). Facies, cycles, and controls on the evolution of a keep-up carbonate platform (Kimmeridgian, Swiss Jura). *Sedimentology*, *52*(6), 1207–1227. doi:10.1111/j.1365-3091.2005.00736.x

Comment, G., Lefort, A., Koppka, J., & Hantzpergue, P. (2015). Le Kimméridgien d'Ajoie (Jura, Suisse) : Lithostratigraphie et biostratigraphie de la Formation de Reuchenette. *Revue de Paléobiologie*, *34*, 161–194.

D'Orazi Porchetti, S., Bernardi, M., Cinquegranelli, A., Dos Santos, V. F., Marty, D., Petti, F. M., Caetano, P. S., & Wagensommer, A. (2016). A review of the dinosaur track record from Jurassic and Cretaceous shallow marine carbonate depositional environments. In P. L. Falkingham, D. Marty, & A. Richter (Eds.), *Dinosaur tracks: The next steps* (pp. 380–390). Indiana University Press.

Davidson, J. B., Farlow, J. O., Green, T. L., & Mallon, J. C. (2025). Testing the utility of interdigital angle as a taxonomically informative variable in tridactyl dinosaur ichnology. *Italian Journal of Geosciences*, *144*(3), 364–387. doi:10.3301/IJG.2025.16

Dercourt, J., Ricou, L. E., & Vrielynck, B. (1993). *Atlas of Tethys*. CCGM/CGMW.

Enay, R. (2000). Recalage biostratigraphique et nouvelle datation de surfaces d'emersion du Kimmeridgien-Tithonien dans le Jura meridional et consequences sur leur interpretation sequentielle. *Bulletin de la Société Géologique de France*, *171*(6), 665–671. doi:10.2113/171.6.665

Enriquez, N. J., Campione, N. E., Brougham, T., Fanti, F., White, M. A., Sissons, R. L., Sullivan, C., Vavrek, M. J., & Bell, P. R. (2020). Exploring possible ontogenetic trajectories in tyrannosaurids using tracks from the Wapiti Formation (upper Campanian) of Alberta, Canada. *Journal of Vertebrate Paleontology*, *40*(6), e1878201. doi:10.1080/02724634.2021.1878201

Foster, J. R., Harris, J. D., Milner, A. R. C., Bordy, E. M., Sciscio, L., Castanera, D., Belvedere, M., Xing, L., & Lockley, M. G. (2024). Jurassic vertebrate tracks and traces. *Vertebrate Ichnology*, 265–478.

Garbuniya, L. K., & Kurbatov, V. V. (1982). Jurassic dinosaur tracks of Tashkurgan (Uzbekistan SSR). In *Abstracts and proceedings of the 23rd Scientific Session* (pp. 20–22). Academy of Sciences of the Georgian Soviet Socialist Republic.

Hallam, A. (2001). A review of the broad pattern of Jurassic sea-level changes and their possible causes in the light of current knowledge. *Palaeogeography, Palaeoclimatology, Palaeoecology*, *167*(1-2), 23–37. doi:10.1016/S0031-0182(00)00229-7

Haq, B. U., Hardenbol, J., & Vail, P. R. (1987). Chronology of fluctuating sea levels since the Triassic. *Science*, *235*(4793), 1156–1167. doi:10.1126/science.235.4793.1156

Jank, M., Meyer, C. A., & Wetzel, A. (2006). Late Oxfordian to late Kimmeridgian carbonate deposits of NW Switzerland (Swiss Jura): Stratigraphical and palaeogeographical implications in the transition area between the Paris Basin and the Tethys. *Sedimentary Geology*, *186*(3-4), 237–263. doi:10.1016/j.sedgeo.2005.08.008

Jank, M., Wetzel, A., & Meyer, C. A. (2006). Late Jurassic sea-level fluctuations in NW Switzerland (late Oxfordian to late Kimmeridgian): Closing the gap between the Boreal and Tethyan realm in Western Europe. *Facies*, *52*(4), 487–519. doi:10.1007/s10347-005-0044-y

Lallensack, J. N., Buchwitz, M., & Romillo, A. (2022). Photogrammetry in ichnology: 3D model generation, visualisation, and data extraction. *Journal of Paleontological Techniques*, *22*, 1–18.

Lallensack, J. N., Engler, T., & Barthel, H. J. (2020). Shape variability in tridactyl dinosaur footprints: The significance of size and function. *Palaeontology*, *63*(2), 203–228. doi:10.1111/pala.12449

Lallensack, J. N., Leonardi, G., & Falkingham, P. L. (2025). Glossary of fossil tetrapod tracks. *Palaeontologia Electronica*, *28*(1), 1–105. doi:10.26879/1389

Le Lœuff, J., Gourrat, C., Landry, P., Hautier, L., Liard, R., Souillat, C., Buffetaut, E., & Enay, R. (2006). A Late Jurassic sauropod tracksite from Southern Jura (France). *Comptes Rendus Palevol*, *5*(5), 705–709. doi:10.1016/j.crpv.2006.01.007

Leonardi, G. (1987). *Glossary and manual of tetrapod footprint*. Publicação do Departemento Nacional da Produzione Mineral.

Li, J. J., Bai, Z. Q., & Wei, Q. Y. (2011). *On the dinosaur tracks from the Lower Cretaceous of Otog Qi, Inner Mongolia*. Geological Publishing House.

Li, Y., Jiang, S., & Wang, X. (2020). The largest species of *Asianopodus* footprints from Junggar Basin, Xinjiang, China. *Chinese Science Bulletin*, *65*(18), 1875–1887. doi:10.1360/TB-2019-0513

Lockley, M. G. (2009). New perspectives on morphological variation in tridactyl footprints: Clues to widespread convergence in developmental dynamics. *Geological Quarterly*, *53*(4), 415–432.

Lockley, M., Gierlinski, G. D., & Lucas, S. G. (2011). *Kayentapus* revisited: Notes on the type material and the importance of this theropod footprint ichnogenus. *New Mexico Museum of Natural History and Science Bulletin*, *53*, 330–336.

Lockley, M. G., Meyer, C. A., & dos Santos, V. F. (1996). *Megalosauripus*, *Megalosauropus* and the concept of megalosaur footprints. *The Continental Jurassic.Museum of Northern Arizona Bulletin*, *60*, 113–118.

Lockley, M. G., Meyer, C. A., & dos Santos, V. F. (1998). *Megalosauripus* and the problematic concept of megalosaur footprints. *GAIA*, *15*, 313–337.

Lockley, M. G., Meyer, C. A., Schultz-Pittman, R., Forney, G., & Morales, M. (1996). Late Jurassic dinosaur tracksites from Central Asia: A preliminary report on the world's longest trackways. *Museum of Northern Arizona Bulletin*, *60*, 137–140.

Lucas, S. G., Hunt, A. P., & Klein, H. (2024). *Vertebrate Ichnology: Tetrapod Tracks and Trackways*. Elsevier.

Mallison, H., & Wings, O. (2014). Photogrammetry in paleontology: A practical guide. *Journal of Paleontological Techniques*, *12*, 1–31.

Mangold, C., & Enay, R. (2004). *Notice explicative: Carte géol. France (1/ 50 000 | feuille Nantua 652)*. Bureau de Recherches Géologiques et Minières.

Marchetti, L., Belvedere, M., Voigt, S., Klein, H., Castanera, D., Díaz-Martínez, I., Marty, D., Xing, L., Feola, S., Melchor, R. N., & Farlow, J. O. (2019). Defining the morphological quality of fossil footprints. Problems and principles of preservation in tetrapod ichnology with examples from the Palaeozoic to the present. *Earth-Science Reviews*, *193*, 109–145. doi:10.1016/j.earscirev.2019.04.008

Marty, D. (2008). Sedimentology, taphonomy, and ichnology of Late Jurassic dinosaur tracks from the Jura carbonate platform (Chevenez-Combe Ronde tracksite, NW Switzerland): Insights into the tidal-flat palaeoenvironment and dinosaur diversity, locomotion, and palaeoecology. *GeoFocus*, *21*, 1–278.

Marty, D., Becker, D., Braillard, L., Ayer, J., Berger, J.-P., Billon-Bruyat, J.-P., Hug, W. A., & Meyer, C. A. (2007). Late Jurassic dinosaur tracksites of the Transjurane highway (Canton Jura, NW Switzerland): Overview and measures for their protection and valorisation. *Bulletin für Angewandte Geologie*, *12*(2), 75–89.

Marty, D., Belvedere, M., Razzolini, N. L., Lockley, M. G., Paratte, G., Cattin, M., Lovis, C., & Meyer, C. A. (2018). The tracks of giant theropods (*Jurabrontes curtedulensis* ichnogen. & ichnosp. nov.) from the Late Jurassic of NW Switzerland: palaeoecological & palaeogeographical implications. *Historical Biology*, *30*(7), 928–956. doi:10.1080/08912963.2017.1324438

Matsukawa, M., Shibata, K., Kukihara, R., Koarai, K., & Lockley, M. G. (2005). Review of Japanese dinosaur track localities: Implications for ichnotaxonomy, paleogeography and stratigraphic correlation. *Ichnos*, *12*(3), 201–222. doi:10.1080/10420940591009231

Mazin, J. M., Hantzpergue, P., & Olivier, N. (2017). The dinosaur tracksite of Plagne (early Tithonian, Late Jurassic; Jura Mountains, France): The longest known sauropod trackway. *Geobios*, *50*(4), 279–301. doi:10.1016/j.geobios.2017.06.004

Mazin, J. M., Hantzpergue, P., & Pouech, J. (2016). The dinosaur tracksite of Loulle (early Kimmeridgian; Jura, France). *Geobios*, *49*(3), 211–228. doi:10.1016/j.geobios.2016.01.018

Meyer, C. A. (2011, April 14-17). *The hitch-hikers guide to the Late Jurassic and Early Cretaceous: Dinosaur tracks from the Swiss and French Jura Mountains in a sequence stratigraphic* [Paper presentation]. Dinosaur Track Symposia 2011, Obernkirchen, Germany.

Meyer, C. A., & Lockley, M. G. (1997). Jurassic and Cretaceous dinosaur tracksites from Central Asia (Usbekistan and Turkmenstan). *Paleontological Society of Korea Special Publication*, *2*, 77–92.

Meyer, C. A., & Lockley, M. (1996). The Late Jurassic continental record of northern Switzerland: Evidence and implications. *The Continental Jurassic (Museum of Northern Arizona Bulletin*, *60*, 421–426.

Meyer, C. A., & Marty, D. (2014). The recurrent record of terrestrial environments in the Late Jurassic of the Swiss Jura mountains: Implications for paleogeographic reconstructions. In E. Maxwell, & J. Miller-Camp (Eds.), *Abstracts of papers: 74th annual meeting, Berlin* (pp. 187). Society of Vertebrate Paleontology.

Meyer, C. A., & Thüring, B. (2003). Dinosaurs of Switzerland. *Comptes Rendus Palevol*, *2*(1), 103–117. doi:10.1016/S1631-0683(03)00005-8

Olsen, P., Smith, J., & McDonald, N. (1998). Type material of the type species of the classic theropod footprint genera *Eubrontes*, *Anchisauripus*, and *Grallator* (Early Jurassic, Hartford and Deerfield basins, Connecticut and Massachusetts, U.S.A.). *Journal of Vertebrate Paleontology*, *18*(3), 586–601. doi:10.1080/02724634.1998.10011086

R Core Team. (2023). *R: A language and environment for statistical computing. R Foundation for Statistical Computing* [Computer software]. https://www.R-project.org/

Razzolini, N. L., Oms, O., Castanera, D., Vila, B., Santos, V. F. Dos, & Galobart, À. (2016). Ichnological evidence of Megalosaurid Dinosaurs Crossing Middle Jurassic Tidal Flats. *Scientific Reports*, 6, 1–15. https://doi.org/10.1038/srep31494

Razzolini, N. L., Belvedere, M., Marty, D., Paratte, G., Lovis, C., Cattin, M., & Meyer, C. A. (2017). *Megalosauripus transjuranicus* ichnosp. nov. A new Late Jurassic theropod ichnotaxon from NW Switzerland and implications for tridactyl dinosaur ichnology and ichnotaxomy. *PLOS One*, *12*(7), e0180289–42. doi:10.1371/journal.pone.0180289

Salisbury, S. W., Romilio, A., Herne, M. C., Tucker, R. T., & Nair, J. P. (2016). The dinosaurian ichnofauna of the Lower Cretaceous (Valanginian–Barremian) Broome Sandstone of the Walmadany area (James Price Point), Dampier Peninsula, Western Australia. *Journal of Vertebrate Paleontology*, *36*(sup1), 1–152. doi:10.1080/02724634.2016.1269539

Schindelin, J., Arganda-Carreras, I., Frise, E., Kaynig, V., Longair, M., Pietzsch, T., Preibisch, S., Rueden, C., Saalfeld, S., Schmid, B., Tinevez, J-Y, White, D. J., Hartenstein, V., Eliceiri, K., Tomancak, P., & Cardona, A. (2012). Fiji: An open-source platform for biological-image analysis. *Nature Methods*, *9*(7), 676–682. doi:10.1038/nmeth.2019

Schlager, S. (2017). Morpho and Rvcg: Shape analysis in R: R-packages for geometric morphometrics, shape analysis and surface manipulations. In G. Zheng, S. Li, & G. Székely (Eds.), *Statistical shape and deformation analysis: Methods, implementation and applications* (pp. 217–256). Academic Press.

Sciscio, L., Belvedere, M., Meyer, C. A., & Marty, D. (2022). Sauropod trackway morphometrics: An exploratory study using Highway A16 excavation at the Courtedoux-Tchâfouè Track Site (Late Jurassic, NW Switzerland). *Frontiers in Earth Science*, *10*, 1–19. doi:10.3389/feart.2022.805442

Sciscio, L., Meyer, C. A., Fara, E., Landry, P., Moreau, J.-D., & Olivier, N. (2025). Differentiating sauropod from thyreophoran tracks: insights from the Late Jurassic Villette Tracksite (Jura, France). *Italian Journal of Geosciences*, *144*(3), 388–404. doi:10.3301/IJG.2025.17

Strasser, A. (2022). Shallow marine carbonates as recorders of orbitally induced past climate changes – example from the Oxfordian of the Swiss Jura Mountains. *Climate of the Past*, *18*(9), 2117–2142. doi:10.5194/cp-18-2117-2022

Thulborn, R. A. (1990). *Dinosaur tracks*. Chapman and Hall.

Thulborn, T. (2001). History and nomenclature of the theropod dinosaur tracks *Bueckeburgichnus* and *Megalosauripus*. *Ichnos*, *8*(3-4), 207–222. doi:10.1080/10420940109380188

Waite, R., Marty, D., Strasser, A., & Wetzel, A. (2013). The lost paleosols: Masked evidence for emergence and soil formation on the Kimmeridgian Jura platform (NW Switzerland). *Palaeogeography, Palaeoclimatology, Palaeoecology*, *376*, 73–90. doi:10.1016/j.palaeo.2013.02.020

Xing, L., Lockley, M. G., Mao, Z., Klein, H., Gu, Z., Bai, C., Qiu, L., Liu, Y., Romilio, A., Persons, W. S., & Wan, X. (2021). A new dinosaur track site from the earliest Cretaceous (Berriasian) part of the Tuchengzi Formation, Hebei Province, China: Implications for morphology, ontogeny and paleocommunity structure. *Palaeogeography, Palaeoclimatology, Palaeoecology*, *580*(110619), 110619–20. doi:10.1016/j.palaeo.2021.110619

Handling Editor: Steven Salisbury.